Effect of spatial sampling on pattern noise in insect-based motion detection

Sreeja Rajesh, Andrew Straw, David C. O'Carroll, Derek Abbott

Sreeja Rajesh, Andrew Straw, David C. O'Carroll, Derek Abbott, "Effect of spatial sampling on pattern noise in insect-based motion detection," Proc. SPIE 5649, Smart Structures, Devices, and Systems II, (28 February 2005); doi: 10.1117/12.598178

SPIE.

Event: Smart Materials, Nano-, and Micro-Smart Systems, 2004, Sydney, Australia

Effect of spatial sampling on pattern noise in insect-based motion detection

Sreeja Rajesh[a,b,c], Andrew Straw[b,c,d], David O'Carroll[a,b,c] and Derek Abbott[a,c]

[a]School of Electrical & Electronic Engineering, The University of Adelaide, SA 5005, Australia.
[b]School of Molecular and Biomedical Science, The University of Adelaide, SA 5005, Australia.
[c]Centre for Biomedical Engineering, The University of Adelaide, SA 5005, Australia.
[d]Dickinson Lab, California Institute of Technology, Pasadena, CA 91125, USA.

ABSTRACT

Insects perform highly complicated navigational tasks even though their visual system is relatively simple. The main idea of work in this area is to study the visual system of insects and to incorporate algorithms used by them in electronic circuits to produce low power, computationally simple, highly efficient, robust devices capable of accurate motion detection and velocity estimation. The Reichardt correlator model is one of the earliest and the most prominent biologically inspired models of motion detection developed by Hassentein and Reichardt in 1956. In an attempt to get accurate estimates of yaw velocity using an elaborated Reichardt correlator, we have investigated the effect of pattern noise (deviation of the correlator output resulting from the structure of the visual scene) on the correlator response. We have tested different sampling methods here and it is found that a circular sampled array of elementary motion detectors (EMDs) reduces pattern noise effectively compared to an array of rectangular or randomly selected EMDs for measuring rotational motion.

Keywords: Reichardt correlator, pattern noise, spatial sampling, artificial insect vision.

1. INTRODUCTION

Models of the visual systems of insects, with their relative simplicity and efficiency, have become the building blocks for improving the various techniques used in motion detection and velocity estimation. Of the various models of motion detection based on insect vision, the earliest and the most prominent model is the Reichardt correlator model which was developed by Hassenstein and Reichardt in 1956.[1]

The Reichardt correlation motion detector possess a highly parallel architecture. Each elementary motion detector (EMD) detects motion in a preferred direction by comparing a signal from one receptor with a delayed signal from an adjacent receptor. The comparison is performed using a nonlinear, multiplicative interaction between the two channels. Two EMDs tuned to opposite directions are combined to form a bidirectional motion detector.[2]

Most of the spatiotemporal energy models, the dominant models for motion detection in vertebrates, are mathematically equivalent to correlator models.[3] Correlator models have been applied to explain motion detection in humans, birds and cats.[4–6] Though insects and humans are capable of estimating image velocities,[7,8] the basic correlator model does not function as a velocity estimator. It reliably indicates directional

Further author information: (Send correspondence to Sreeja Rajesh)
Sreeja Rajesh: e-mail: srajesh@eleceng.adelaide.edu.au, Telephone: 8303-6296
Andrew Straw: e-mail: astraw@caltech.edu
David O'Carroll: e-mail: david.ocarroll@adelaide.edu.au
Derek Abbott: e-mail: dabbott@eleceng.adelaide.edu.au

Smart Structures, Devices, and Systems II, edited by Said F. Al-Sarawi,
Proceedings of SPIE Vol. 5649 (SPIE, Bellingham, WA, 2005)
0277-786X/05/$15 · doi: 10.1117/12.598178

motion of sinusoidal gratings, but the response depends on contrast (brightness) and spatial frequency (shape) as well as velocity.[9] Analysis and simulations suggest that the processes commonly found in visual systems, such as pre-filtering, response compression, integration, and adaptation, improve the reliability of velocity estimation and expand the range of velocities coded.[10–16] Hence we have elaborated the basic Reichardt model to mimic the properties of the insect visual system.[2] We have not included motion adaptation in our elaborated model here, in order to simplify the error analysis.

The errors considered here in this paper are due to 'pattern noise', the deviation in correlator output that results from the structure of the visual scene. Physiological motion detectors also suffer from random noise, which is due to the variation in its response on repeated presentation of identical stimulus patterns. The random noise experienced by a biological motion detector falls into two categories, namely photon noise and intrinsic noise. The photon noise results from variations in the number of photons absorbed by a photoreceptor in a given unit of time. In addition, the neurons and synapses that comprise the correlator generate intrinsic noise. Studies done on the LMCs (Lamina Monopolar Cells) by Laughlin[11] indicates that photon noise dominates intrinsic noise up to moderate light intensities and at higher light intensities, photon noise equals intrinsic noise in magnitude.

Dror conducted studies on photon noise using Aiken's images and found that while photon noise leads to a slight increase in relative error, its contribution is small compared to that of pattern noise suggesting that the performance of a velocity estimation system based on Reichardt correlators depends primarily on responses to pattern noise.[17]

The accuracy in the estimation of the motion parameters depends largely on the field of view.[18] When the diameter of the receptive field is small, the nature of the field line pattern becomes unclear and there can be no decision of whether a field is due to translation or due to rotation or a mixture of both.[18] The tangential neurons on the fly brain are sensitive to the typical optic flow patterns generated during self-motion. It was found that a simplified linear model of these neurons which performs sampling from large receptive fields can be used to estimate self-motion from optic flow.[19]

In this paper, we have experimented with different spatial sampling techniques in a correlation based system to understand their effect on pattern noise. It was found that a circular array of EMDs reduces pattern noise compared to a rectangular grid of EMDs or randomly selected EMDs for measuring rotational velocity, indicating that the circular method of sampling the detectors may be optimal for creating yaw detectors.

2. VISUAL SYSTEM OF INSECTS

Flying insects depend mainly on retinal motion patterns to control and stabilise their course of motion. The visual information obtained by the photoreceptors is conveyed by the receptor axons in the optic lobe, which consists of successive visual neuropils namely lamina, medulla, lobula and lobula plate as shown in Figure 1. Each visual neuropil is composed of retinotopically arranged columns and superimposed layers. Columns are built up by parallel centripetal and centrifugal small field neurons. The centripetal output cells of the lobula plate project into the brain and the centrifugal cells project from the brain into the lobula plate. Output connections from the optic lobe to the brain are established by both columnar and tangential cells. Columnar cells leave the lobula and the lobula plate as dense bundles and terminate in visual centres of the ventrolateral brain termed optic foci. Tangential output neurons of the optic lobe originate from all the neuropils except the lamina. Some of them connect both the optic lobes (heterolateral elements) and others project also into the optic foci. The optic foci can be regarded as the major sensory integration areas for the motor control in the brain.[14] Apart from the optic lobes, they also receive information from the ocelli, and mechanosensory inputs from the antenna and the halteres. The output elements of these are descending neurons, which pass through the cervical connective and terminate in the motor neuropils of the thoracic ganglion.[14]

The main motion computation centre in the whole pathway is the lobula plate. The lobula plate receives input from the columnar cells derived from the medulla and lobula. Typical output elements of the lobula plate are two classes of giant neurons termed the horizontal system (HS) and vertical system (VS). The horizontal

system consists of three elements, the dendritic arbours of which are located near the anterior surface of the neuropil. According to these dendritic locations, the three cells are termed north, equatorial and south horizontal cells (HSN, HSE and HSS). The three HS neurons (HSN, HSE and HSS) together occupy the whole retinotopic area of the lobula plate. Each of them covers roughly one third of the dorsoventral extent of the neuropil with some overlap. Correspondingly, their receptive field covers the dorsal, equatorial and ventral areas of the ipsilateral visual hemisphere. The dendrites of the HS neurons arborize in the anterior layers of the lobula plate.[20] The vertical cells are a class of 11 output neurons (VS1-11), also occupying the whole retinotopic area of the lobula plate. Their dendritic fields are more strip-like and oriented dorsoventrally. The dendrites are stacked from distal to the proximal side of the lobula plate and overlap considerably.[21, 22]

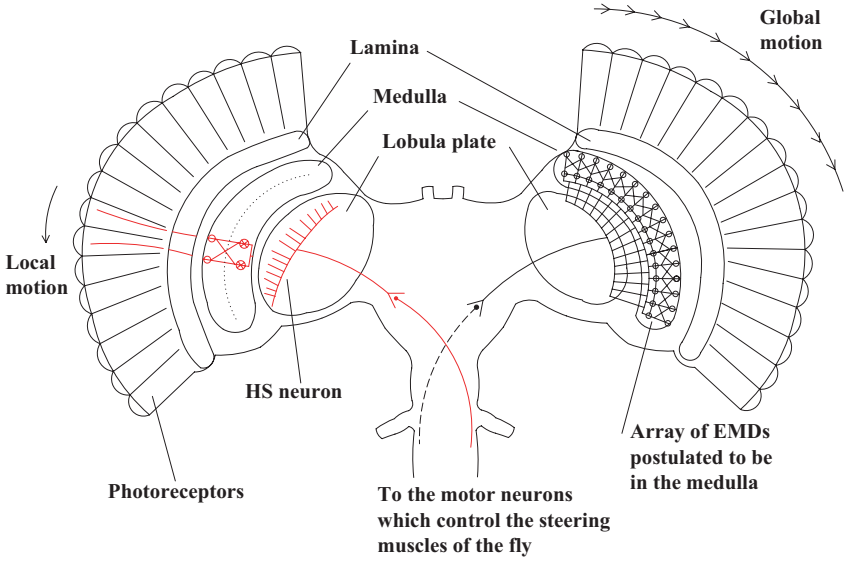

Figure 1. The visual system of insects showing the early visual pathways projecting from the photoreceptors to the visual neuropils namely the lamina, medulla, lobula and the lobula plate. The visual information is passed from the photoreceptors to the lamina and motion is detected by the EMDs in the medulla. The various motion detecting interneurons in the lobula plate (the lighter colored line in the figure shows the example of a HS neuron) passes on the information through the optic foci to the brain which then sends the information through the descending interneurons to the motor neurons, which control the steering muscles thereby enabling flight control in insects.

Optomotor yaw torque responses are selectively induced by horizontal motion[23, 24] and hence must be controlled by EMDs having sampling bases parallel to the horizontal axis of the eye lattice or by pairs of EMDs having symmetrically arranged sampling bases with respect to the axis, the outputs of which are added together. Monocular stimulation with progressive (front to back) motion leads to a simultaneous decrease of the ipsilateral and an increase of the contralateral wing beat amplitude and thus to the generation of yaw torque turning the animal in the same direction as the perceived motion. Regressive (back to front) motion is less effective but leads to syndirectional torque responses. Horizontal motion activates two motion sensitive systems behind each eye, which integrate the output of the arrays of the EMDs and that are specifically tuned to large field motion (global motion) and small field motion or object motion (local motion). The large field system is activated by ipsilateral front to back and contralateral back to front motion, and induces syndirectional yaw

torque responses of the fly by simultaneous excitation and inhibition of the contralateral and ipsilateral flight motor respectively. The small field system is activated by the ipsilateral horizontal motion of small objects in both directions and induces turning towards the stimulus. The output channels of the small field and large field systems contain different frequency filters. The small field and large field systems dominate in torque-control under stimulation with high frequency and low frequency oscillatory motion respectively.[25] Since under natural conditions, the rotatory retinal motion patterns arise from self rotations of the animal in space, HS system appears to act as a visual yaw-monitor, specifically designed for the control of course-stabilising yaw torque generation by the motor system.[14, 26]

The motion sensitive cells of the lobula plate supply input to the flight control system. The visual system, however, is not the only sensory modality that detects self-motion during flight. Mechanosensory fields at the base of the of the beating halteres detect forces that result when the fly rotates in space.[27] These gyroscopic sensors are more effective in detecting high speed body rotations and mediate the reflexive changes in the wing kinematics that stabilize the animal against mechanical perturbations during flight, while the slower rotations or drift during flight is more easily detected by the visual system. Thus these two sensory modalities encode different ranges of oscillation frequencies over which the animal operates. The halteres, like aerodynamically active forewings, are equipped with their own set of steering muscles, which receives strong excitory input from descending visual interneuron.[28] Some haltere afferents form mono-synaptic electrical synapses with steering muscle motor neurons. This control loop of visual feedback to haltere muscles, and haltere feedback to wing muscles allows the visual system to initiate responses in wing steering muscles indirectly or to control the gain of haltere mediated reflexes, thus enabling flight control in insects.[29, 30]

3. PRESENCE OF PATTERN NOISE

Differences in the structure of scenes result in variations in the correlator response termed as the pattern noise. In order to clearly demonstrate this, physiological and modelling experiments were done at a high speed and at a low speed by repeating the same stimulus at the same and different initial positions.

3.1. Electrophysiology methods

Males of the fly *Eristalis tenax* were captured in the wild and the membrane potential of wide-field motion detecting neurons (HS cells) was recorded intracellularly using standard techniques.[31]

Stimuli were presented on a CRT display (Flatron 915 FT Plus, LG Electronics) at a frame rate of 200 Hz at 640 by 480 pixel resolution and mean luminance of 41 cd/m^2. A conventional OpenGL graphics card (geForce 3 Ti 200, nVidia) was used with Vision Egg stimulus generation software by author Andrew Straw (www.visionegg.org). The stimuli used were the same digital panoramas used for the modeling experiments. These panoramas were presented on the inside of a virtual cylinder, which was centered on the fly and perspective distorted according to the fly's calibrated 3D position and orientation relative to the screen. Motion simulated pure yaw rotations by spinning the virtual cylinder about the dorsal-ventral axis of the fly's head. The display subtended approximately 90 degrees horizontally from midline to the lateral portion of the animal, thus stimulating most of the receptive field of HS neurons.[20, 32]

3.2. Electrophysiology results

By aligning responses in time across several initial stimulus positions, both pattern noise and intrinsic noise is largely removed from the mean, but both contribute to the standard deviation ('time aligned' in Figure 2 and 3). When responses are aligned by stimulus position ('phase aligned'), the mean is subject to pattern noise while the standard deviation indicates only intrinsic noise. A comparison of the mean between time aligned and phase aligned responses shows the presence of pattern noise on real HS cells in our experimental setup. The larger standard deviation of the time aligned response compared to the phase aligned response indicates that pattern noise greatly exceeds intrinsic noise in HS cells at 850 deg/sec. Unfortunately, our recording durations were too short to perform the same phase alignment at 100 degrees per second, but inspection of the individual responses indicates that pattern noise is less significant at this slower speed.

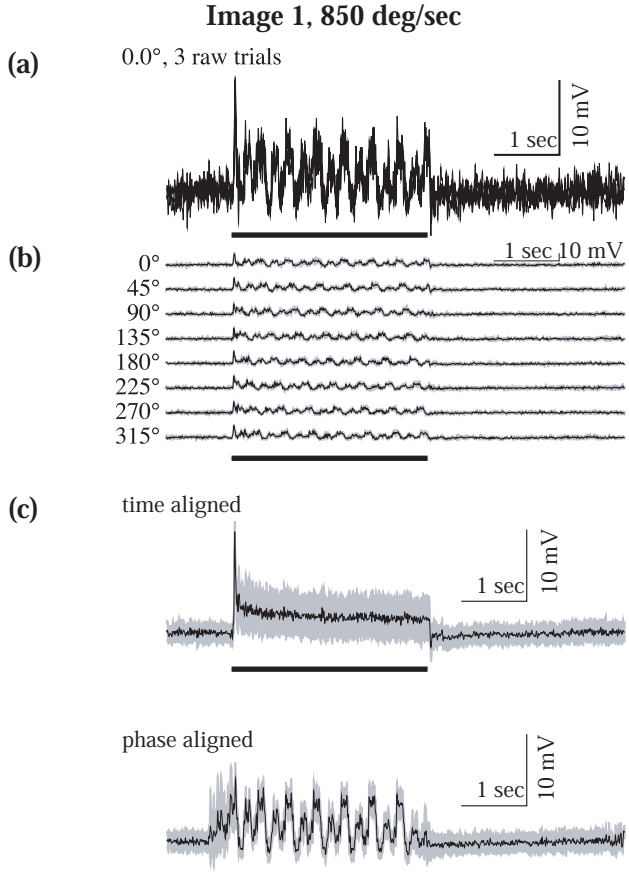

Figure 2. This figure shows the effect of 'pattern noise' on response of a single fly wide-field motion detecting neuron (HS cell) to image 1 (see Figure 6), with the image presented moving at 850 degrees per second at 8 different initial phases, each 45 degrees apart. For each combination of velocity and image, part (a) shows three responses to identical experimental conditions. Part (b) shows the mean of at least three responses at each of several stimulus positions. Part (c) show the mean response in black and the standard deviation of the response around the mean in gray. The 'time aligned' response shows the individual responses at each initial position averaged without compensating for position change. For the 850 degree/second motion, responses were also 'phase aligned' by compensating for the position change before averaging. To eliminate noisy high frequency signal components, signals were low pass filtered before averaging.

3.3. Modelling results

Figure 4 and Figure 5 shows the response of our elaborated EMD model[2] designed with an EMD averaging window, the same angular size as the computer screen used for the physiological experiment, and the simulation is run at the same speed as done in the physiological experiment (850°/sec and 100 degrees per second) using the same eight phases. The results obtained at phase zero and at each different initial phase are shown and it can be seen that it is similar to the physiological results clearly showing the pattern noise present. Since intrinsic noise is totally absent in the model, the noise present is mainly caused by the pattern noise. Then as carried out before, the resulting 8 curves are averaged in two ways, (i) time aligned and (ii) phase aligned. The response of the model agrees well with the physiological results clearly demonstrating that the pattern noise is indeed a major source of temporal response variation in real HS recordings. It is also seen from both physiological and modelling results that pattern noise is present more significantly at higher speeds.

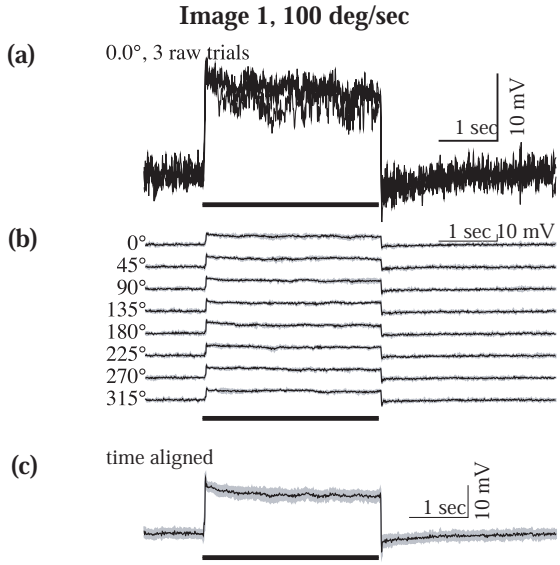

Figure 3. This figure shows the effect of 'pattern noise' on response of a single fly wide-field motion detecting neuron (HS cell) to image 1 (see Figure 6), with the image presented moving at 100 degrees per second at 8 different initial phases, each 45 degrees apart. For each combination of velocity and image, part (a) shows three responses to identical experimental conditions. Part (b) shows the mean of at least three responses at each of several stimulus positions. Part (c) show the mean response in black and the standard deviation of the response around the mean in gray. The 'time aligned' response shows the individual responses at each initial position averaged without compensating for position change. Unfortunately, our recording durations were too short to perform the same phase alignment at 100 degrees per second, but inspection of the individual responses indicates that pattern noise is less significant at this slower speed. To eliminate noisy high frequency signal components, signals were low pass filtered before averaging.

4. SAMPLING OF THE EMDS

Our hypothesis is that the large strip-like nature of the HS cell receptive field, which is fully circular if summation at the steering muscles is taken into account, plays a functional role in encoding velocity. Because the circular array of EMDs is parallel to the preferred direction of motion, a purely circular optical flow pattern (i.e. yaw for an HS neuron) would produce the same temporal sequence of stimulation of individual photoreceptors. Hence if a high contrast feature is present within the receptive field at one point in time, it will also be present at future times. By summing across such an array, pattern noise is largely reduced.

In order to test this hypothesis, we ran simulations with a panoramic yaw stimulus with a fixed velocity, for 2 seconds. We ran the test for 4 different panoramic images (these images are shown in Figure 6) and 12 different speeds for each. We then sampled the matrix of EMD outputs in one of 4 ways.

The four ways in which we have sampled the output of the EMDs are

1) the output of all the EMDs are used which we call as total, as we have used all our EMDs here, 2) the output of a randomly selected rectangular array of 15×16 EMDs are taken in this case, 3) the output of randomly selected 240 EMDs from the total sample of EMDs are used, 4) And finally the response of a randomly selected circular row of 240 EMDs is taken.

Each case is clearly explained in the subsections below.

4.1. Total sample of all EMDs

The first (labelled 'total' in the figures below) is the sum (across the time dimension) of all EMDs. Here we have sampled the outputs of the all EMDs (240×37 EMDs). In this method, the outputs of all the EMDs

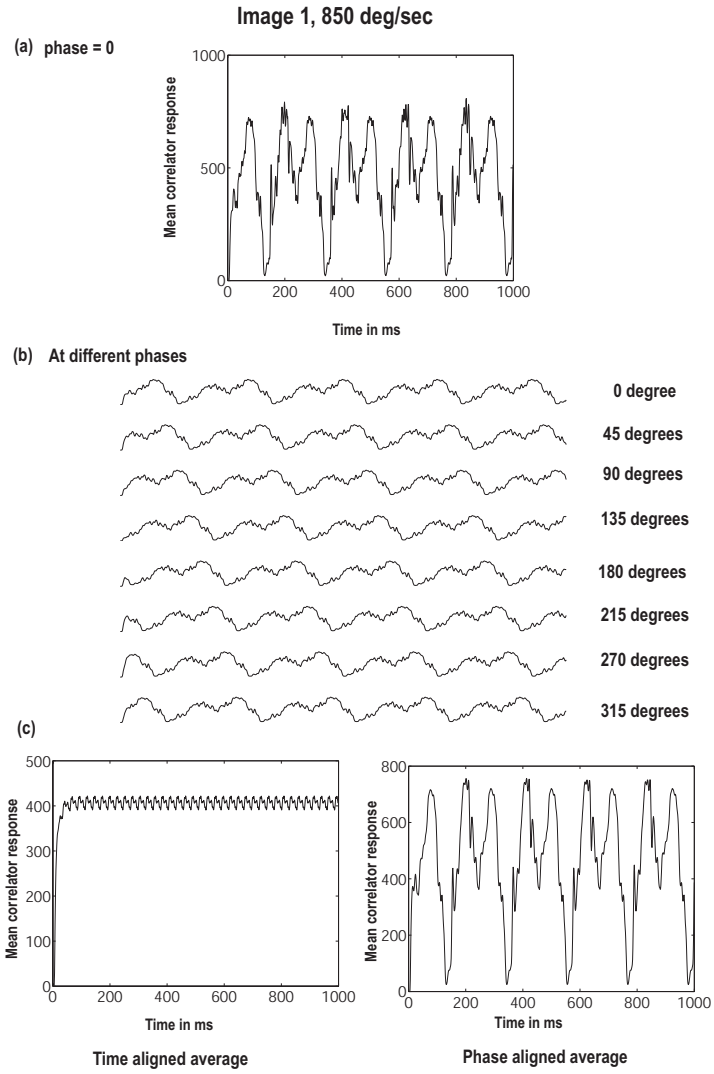

Figure 4. This figure shows the simulation results obtained by running the model at 850 degrees per sec using the same image, at 8 different initial phases, each 45 degrees apart, as done in the physiological experiment shown in Figure 2. Part (a) of the graph shows the response at phase zero. Part (b) shows the response to each of the 8 configurations. Part (c) shows the response averaged in the time aligned way. In the time aligned method, the normal average of the each of the eight response removes the pattern noise as the response is aligned by stimulus time. The results obtained agree with the physiological data, demonstrating that pattern noise acts as a major source of temporal response variation in HS recording

are averaged over time where as in the forthcoming sections only selected EMDs are used from the total array and the effect of each of these sampling techniques on the pattern noise is noted by calculating the relative error which is clearly explained in the next section.

4.2. Square lattice

A randomly selected rectangular grid of 15×16 EMDs (i.e 240 total) as shown in Figure 8 is used here. Since sampling of a square array of detectors gives a similar response, it can even be called a square lattice as is referred to in this paper.

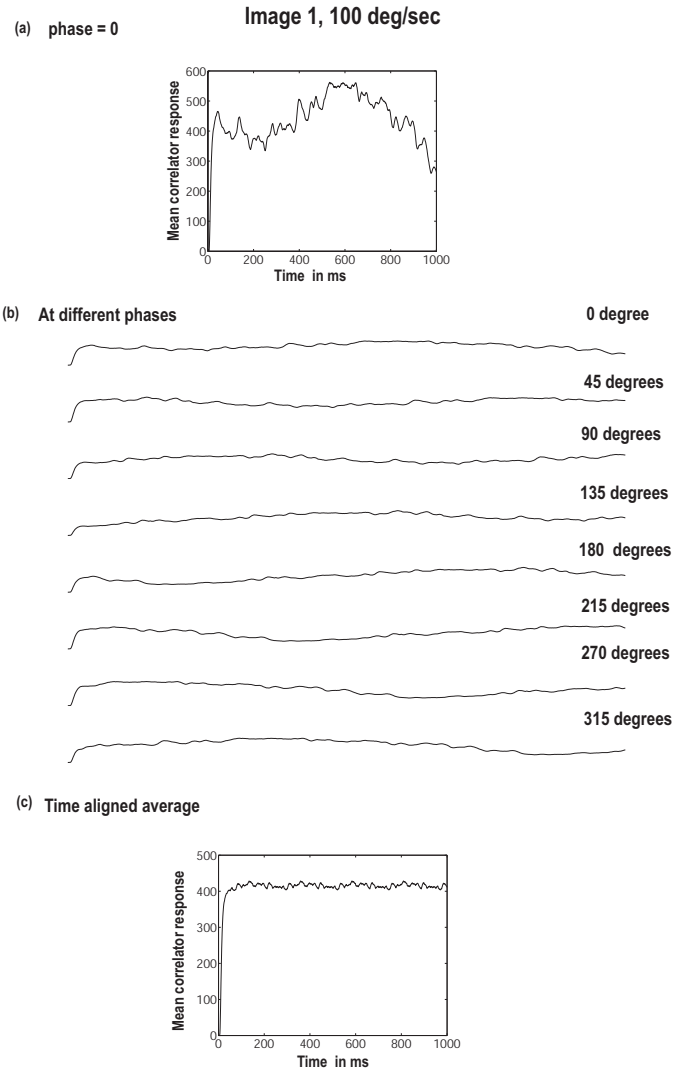

Figure 5. This figure shows the simulation results obtained by running the model at 100 degrees per sec using the same image, at 8 different initial phases, each 45 degrees apart, as done in the physiological experiment shown in Figure 3. Part (a) of the graph shows the response at phase zero. Part (b) shows the response to each of the 8 configurations. Part (c) shows the response averaged in two ways, time aligned and phase aligned. In the time aligned method, the normal average of the each of the eight response removes the pattern noise as the response is aligned by stimulus time. In the phase aligned method, we align each phase delayed response by shifting each response along the x-axis with the data obtained for phase zero and then we average it. Now the pattern noise is still present because in this way, it is the image position that is averaged rather than time, and we can still see the noise as the noise is locked in the stimulus position. The results obtained agree with the physiological data, demonstrating that pattern noise acts as a major source of temporal response variation in HS recordings

4.3. Randomly sampled array

In this method, the sample consisted of 240 EMDs selected randomly from the 240×37 array as shown in Figure 9.

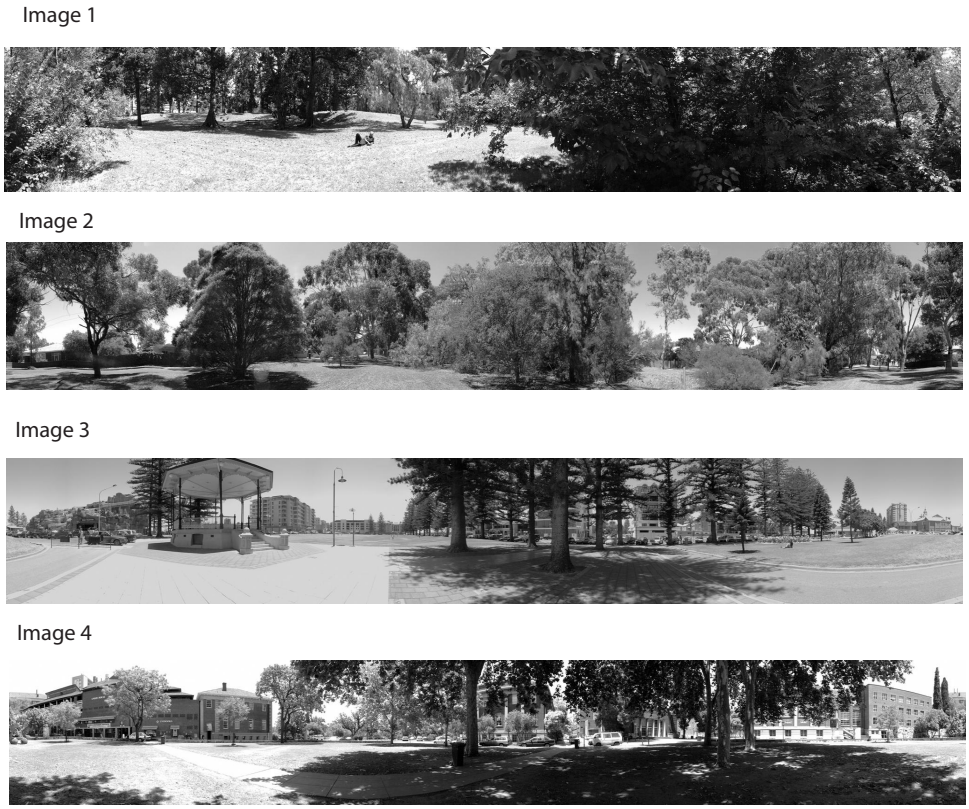

Figure 6. The panoramic images given as stimuli to our model. A panorama of the image is formed by 'warping' 12 image tiles at 30° intervals to remove lens distortions and then by wrapping its ends together using Apple Quicktime VR software on a Macintosh computer.

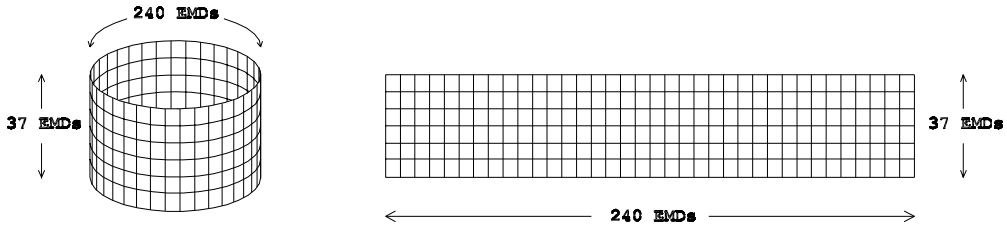

Figure 7. This diagram shows the total array of EMDs (240 × 37) from which the output of motion detection is logged. The inter-ommatidial angle of 1.5 degrees, which separates each EMD is not shown in this figure. Each box here represents an EMD.

4.4. Circular sampled array

Finally we used a circular linear array with just 240 EMDs, representing one of the 37 possible rows of EMDs, selected at random, as shown in Figure 10.

5. SAMPLING RESULTS

The error measure used here called the relative error defined by Dror as, $E_{rel} = E_{abs}/\overline{R}$, where the absolute error (E_{abs}) is the difference between the actual response and the expected response.[17] The expected response

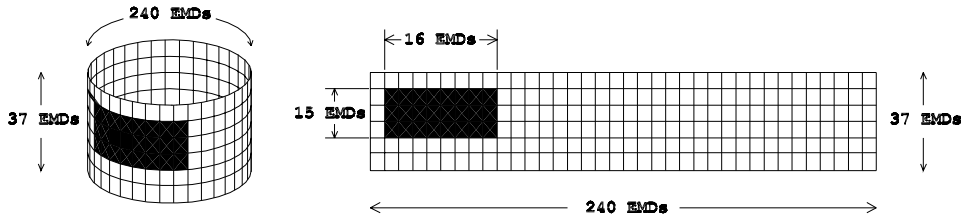

Figure 8. This diagram shows a sample of randomly selected rectangular array of EMDs from which the output of the motion detection is noted. The inter-ommatidial angle of 1.5 degrees, which separates each EMD is not shown in this figure. Each box here represents an EMD and the shaded box represents the EMDs selected from the total array.

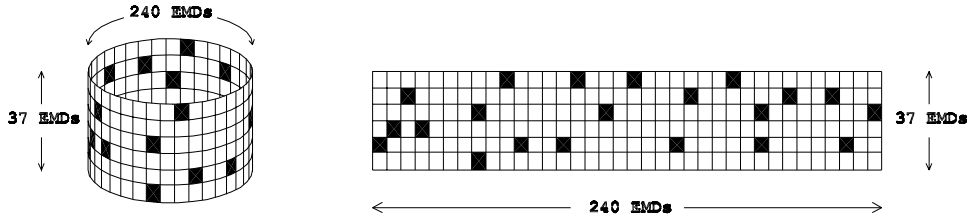

Figure 9. This diagram shows a sample of randomly selected EMDs from the total array of 240×37 EMDs. The inter-ommatidial angle of 1.5 degrees, which separates each EMD is not shown in this figure. Each box here represents an EMD and the shaded box represents the EMDs selected for correlation.

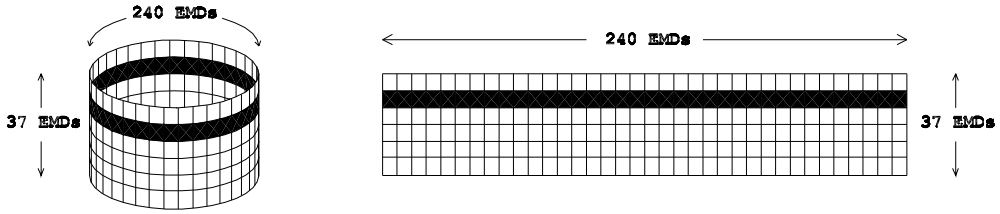

Figure 10. This diagram shows a sample of a randomly selected row of 240 EMDs from which the output of the motion detection is noted. The inter-ommatidial angle of 1.5 degrees, which separates each EMD is not shown in this figure. Each box here represents an EMD and the shaded box represents the EMDs selected for correlation.

is the mean response value that is given by $\overline{R}$. For a given set of images, moving at a given velocity, the mean response $\overline{R}$ is calculated by averaging the response of the wide field correlator at all points in the selected sampled space and sampled time. The relative error for the same set of responses is found by dividing their standard deviation by the mean.

The mean relative error is then calculated for each case (square, circular, random and total) by finding the average relative error for about 20 iterations on all the four images at 12 different speeds and is plotted as shown in Figure 13. It is seen that the relative error of the circular sample of EMDs is less than that of the random sample and the rectangular detector arrays and is much closer to the relative error of the total EMD array. This result suggests that motion detection and velocity estimation at yaw velocity can be done effectively using just a circular array of 240 EMDs.

The error bars in the Figure 11 and the mean correlator response for each case, as shown in Figure 12 also indicate that the circular sample of EMDs reduces errors and pattern noise more than the randomly sampled array and rectangular or square grid of EMDs.

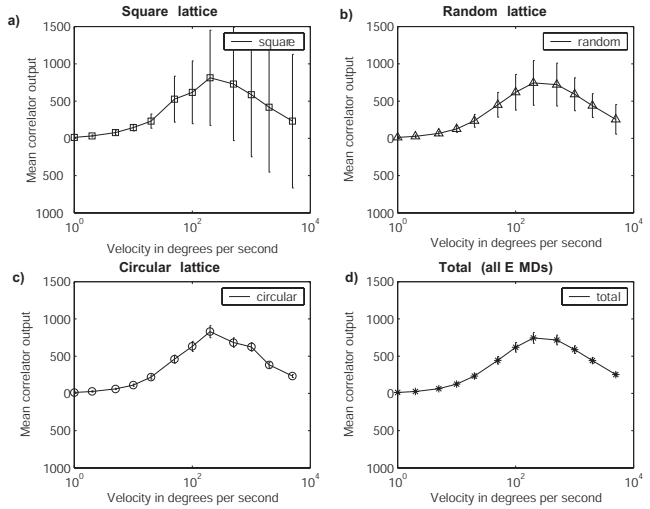

Figure 11. (a) Responses and relative error obtained from the simulation of a rectangular array (16×15) array of 240 EMDs. As can be seen the errors in this case indicate that there is more pattern noise when the sampling is done with a rectangular array of EMDs. (b) The error bars are obtained from the simulation of 240 EMDs selected randomly from the total array of 240×37 EMDs. Because of the random selection of the EMDs, we can see some error with this kind of sampling. (c) The error bars are obtained from the simulation of a circular array of 240 EMDs. It is seen that the error in this case is reduced and is similar to using the whole total array of 240×37 EMDs indicating effective encoding of velocity can be done using even a small number of a circular detectors. (d) The error bars obtained from the simulation of total array of 240×37 EMDs. In all four of the above curves, the correlator outputs are given in arbitrary units.

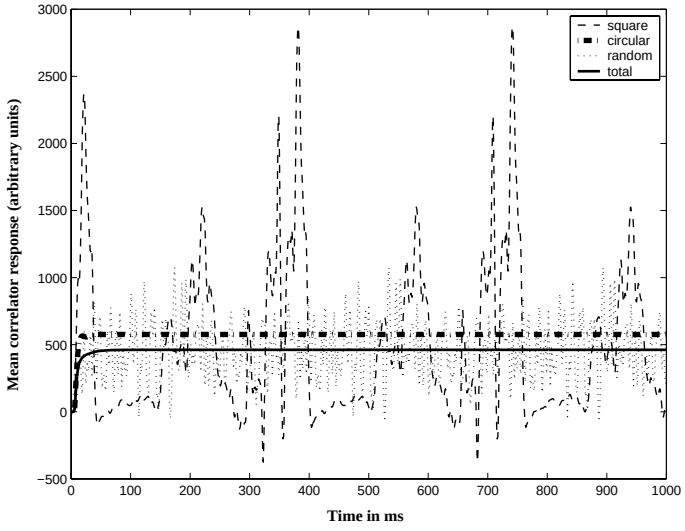

Figure 12. The mean correlator simulated response for the square, circular, random and total array of EMDs for image 1 moving at a constant velocity of 500 degrees per second is shown here. It is seen that the sampling of circular detector array gives a stable output similar to the total sample of EMDs.

6. ROLE OF NATURAL IMAGE STATISTICS

We use natural images as stimuli for our experiments. Natural images are far from random and show a large degree of structure. This structure can be described by the statistics of the image source, and can be consid-

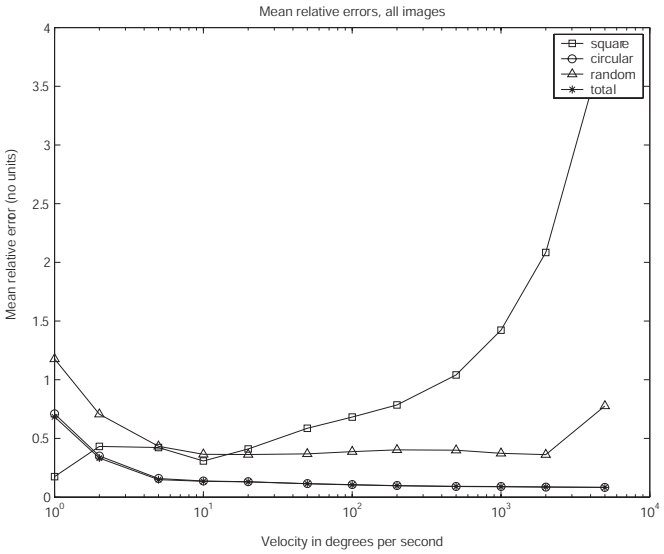

Figure 13. The relative errors obtained from the simulation of the square, random, circular and total array of the EMDs. The relative error defined by Dror as, $E_{rel} = E_{abs}/\overline{R}$, where the absolute error (E_{abs}) is the difference between the actual response and the expected response.[17] The mean relative error is calculated by averaging the relative error obtained for about 20 iterations on all the four images at 12 different speeds. It is clearly seen that the mean relative error for the circular linear array of EMDs is much lower and is closer to that of the total array of detectors.

ered as prior knowledge. Therefore a certain amount of image data is predictable and thus redundant.[33,34] The visual system appears to be optimized to take advantage of the statistical properties of natural images using specific optimization criteria of redundancy minimization, maximisation of information transmission, sparseness of the neural coding and minimising reconstruction error, demonstrating that simple optimisation principles combined with knowledge of image statistics can predict visual processing strategies which are found in nature .[35] Recent development in statistical modelling, along with powerful computational tools, have enabled researchers to study more sophisticated statistical models for visual images and to use them to test the efficient coding hypothesis for both individual neurons and populations of neurons.[36–38] The results of various studies done on the statistics of natural images all draw the same conclusion that the power spectrum of natural images tends to depend on the spatial frequency f in the form of $\frac{1}{f^2}$.

Measured power spectra are one of the most prominent sources of natural image statistics, which are obtained by computing the Fourier transform of an image and multiplying each element of the transform by its complex conjugate. Averaging over horizontal and vertical orientations gives power as a function of frequency. The power spectra of natural images are generally similar. The $\frac{1}{f^2}$ property of natural images is generally not obtained for random images (such as for example, unbiased random noise images, which produce a flat power spectrum). The $\frac{1}{f^2}$ spectral slope of natural images implies that natural images are statistically scale-free.[39] That is, images viewed through different angular scales (through lenses of different focal lengths) have similar statistics.[33–35,40,41]

Studies carried out by Dror reveal that similarities between natural image power spectra lead to predictable peak response velocities and to similarities in the shapes of the velocity response curves for different natural images. The primary difference between the curves, their overall amplitude, results from contrast differences between images. In order to use mean correlator response as a reliable indicator of velocity, the visual system needs to compensate for these contrast variations.[17,40] One possibility is contrast saturation early in the motion detection pathway, which eliminates significant differences in contrast[17] and alternatively some form of adaptation (contrast adaptation) in the visual system, may work to remove contrast difference between the

images.[16, 42] In this paper, we have not included the effects of saturation and adaptation, in order to simplify the model. Future work in this area could be to investigate the effect of these elaborations on pattern noise during simulation of natural images.

7. CONCLUSION

In this paper, we have conducted a study on pattern noise using physiological recordings together with modelling results and we performed quantitative analysis of the effects of receptive field shape on pattern noise, measured as 'relative error'. This error is defined as the residual variance over time in the response due to the local structure of the image, divided by the mean (DC level) of that response. The assumption here is that the DC level of the summed outputs of an EMD (elementary motion detector) array represents the desired velocity signal, while time-variation due to the pattern structure is noise, so that the relative error is effectively a measure of signal-to-noise ratio in the context of the task of velocity coding. It is found that the circular receptive field shape reduces pattern noise compared to an array of rectangular or randomly selected EMDs.

It can also be seen that the circular linear array achieves a very similar variance in velocity estimation to that of the 'full' EMD set, and (depending on speed) 10 or more times lower than the other two strategies for sampling EMDs. We conclude that a circular, linear detector array may be the optimal way to sample outputs from EMDs of the correlator type, at least with respect to reduction of pattern noise when estimating yaw velocity. Taken together with the underlying physiological experiments that are being carried out in our lab, this suggests that a small detector array with as few as 240 pixels could provide robust estimates of speed under natural image conditions. Further, it would be interesting to pursue similar tests on more complex optic flow.

8. ACKNOWLEDGEMENTS

Funding from the US Air force Research Laboratory/Asian Office for Aerospace Research & Development (contract # F62562-01-P-0158), the Sir Ross & Sir Keith Smith Fund and the Australian Research Council is gratefully acknowledged. Andrew D. Straw was supported by a Predoctoral Fellowship from the Howard Hughes Medical Institute.

REFERENCES

1. B. Hassenstein and W. Reichardt, "Structure of a mechanism of perception of optical movement," *Proceedings of the 1st International Conference on Cybernetics* , pp. 797–801, 1956.
2. S. Rajesh, T. Rainsford, and D. C. O'Carroll, "Modelling pattern noise in responses of fly motion detectors to naturalistic scenes," *In this volume* , 2004.
3. E. H. Adelson and J. Bergen, "Spatiotemporal energy models for the perception of motion," *Journal of the Optical Society of America A* **2**, pp. 284–299, 1985.
4. J. P. van Santen and G. Sperling, "Elaborated Reichardt detectors," *Journal of the Optical Society of America A* **2**, pp. 300–321, 1985.
5. F. Wolf-Oberhollenzer and K. Kirschfeld, "Motion sensitivity in the nucleus of the basal optic root of the pigeon," *Journal of Neurophysiology* **71**, pp. 1559–1573, 1994.
6. R. C. Emerson, M. C. Citron, W. J. Vaughn, and S. A. Klein, "Nonlinear directionally selective subunits in complex cells of cat striate cortex," *Journal of Neurophysiology* **58**, pp. 33–65, 1987.
7. M. V. Srinivasan, S. W. Zhang, M. Lehrer, and T. S. Collet, "Honeybee navigation en route to the goal: visual flight control and odometry," *Journal of Experimental Biology* **199**, pp. 237–244, 1996.
8. S. P. McKee, G. H. Silverman, and K. Nakayama, "Precise velocity discrimination despite random variation in temporal frequency and contrast," *Vision Research* **26**, pp. 609–619, 1986.
9. M. Egelhaaf, A. Borst, and W. Reichardt, "Computational structure of a biological motion detection system as revealed by local detector analysis in the fly's nervous system," *Journal of the Optical Society of America A* **6**, pp. 1070–1087, 1989.

10. R. O. Dror, D. C. O'Carroll, and S. B. Laughlin, "Accuracy of velocity estimation by Reichardt correlators," *Journal of the Optical Society of America A* **18**, pp. 241–252, February 2001.
11. S. B. Laughlin, "Matching coding, circuits, cells and molecules to signals: general principles of retinal design in the fly's eye," *Progress in Retinal Research* **13**, pp. 165–195, 1994.
12. M. Egelhaaf and A. Borst, "Transient and steady state response properties of movement detectors," *Journal of the Optical Society of America A* **6**, pp. 116–127, 1989.
13. S. Single and A. Borst, "Dendritic integration and its role in computing image velocity," *Science* **281**, pp. 1848–1850, 1998.
14. K. Hausen and M. Egelhaaf, Neural mechanisms of visual course control in insects, *Facets in vision*, edited by R. Hardie and D. Stavenga, Springer-Verlag, Berlin, 1989.
15. T. Maddess and S. B. Laughlin, "Adaptation of the motion sensitive neuron h1 is generated locally and governed by contrast frequency," *Proceedings of the Royal Society of London B* **225**, pp. 251–275, 1985.
16. R. A. Harris, D. C. O'Carroll, and S. B. Laughlin, "Adaptation and the temporal delay filter of fly motion detectors," *Vision Research* **39**, pp. 2603–2613, 1999.
17. R. O. Dror, "Accuracy of visual velocity estimation by Reichardt correlators," Master's thesis, University of Cambridge, Cambridge, UK, 1998.
18. J. J. Koenderink and A. J. Vandoorn, "Facts on optic flow," *Biological Cybernetics* **54**(4), pp. 247–254, 1987.
19. M. O. Franz and J. S. Chahl, "Insect-inspired estimation of self-motion," *Proceedings of Biologically Motivated Computer Vision, Lecture Notes in Computer Science* **2525**, pp. 171–180, 2002.
20. N. J. Strausfeld and H. S. Seyan, "Convergence of visual, haltere and prosternal inputs at neck motor neurons of *Calliphora erythrocephala*," *Cell and Tissue Research* **240**, pp. 601–615, 1985.
21. H. G. Krapp, B. Hengstenberg, and R. Hengstenberg, "Dendritic structure and receptive field organisation of optic flow processing interneurons in the fly," *Journal of Neurophysiology* **79**, pp. 1902–1917, 1998.
22. M. O. Franz and H. G. Krapp, "Wide-field, motion sensitive neurons and matched filters for optic flow," *Biological cybernetics* **83**, pp. 185–197, 2000.
23. C. Wehrhahn, "Motion sensitive yaw torque response of the housefly *Musca*: A quantitative study," *Biological Cybernetics* **55**, pp. 275–280, 1986.
24. K. Hausen and R. Hengstenberg, "Multimodal convergence of sensory pathways on motor neurons of flight muscles in the fly *Calliphora*," *Society for Neuroscience Abstracts* **13**, p. 1059, 1987.
25. M. Egelhaaf, "Dynamic properties of two control systems underlying visually guided turning in houseflies," *Journal of Comparative Physiology A* **161**, pp. 777–783, 1987.
26. H. Eckert, "The horizontal cells in the lobula plate of the blowfly, *Phaenicia sericata*," *Journal of Comparitive Physiology A* **143**, pp. 511–526, 1981.
27. G. Nalbach and R. Hengstenberg, "The halteres of the blowfly *Calliphora*: Three dimentional organisation of compensatory reaction to real and simulated rotations," *Journal of Comparitive Physiology A* **175**, pp. 695–708, 1994.
28. W. P.Chan, F. Prete, and M. H. Dickinson, "Visual input to the efferent control system of a flys gyroscope," *Science* **280**(5361), pp. 289–292, 1994.
29. M. A. Fyre and M. H. Dickinson, "Fly flight: A model for the neural control of complex behaviour," *Neuron* **32**, pp. 385–388, 2001.
30. R. Hengstenberg, "Controlling the fly's gyroscopes," *Nature* **392**, pp. 757–758, 1998.
31. D. C. O'Carroll, S. B. Laughlin, N. J. Bidwell, and R. A. Harris, "Spatio-temporal properties of motion detectors matched to low image velocities in hovering insects," *Vision Research* **37**, pp. 3427–3439, 1997.
32. K. Hausen, "Motion sensitive interneurons in the optomotor system of the fly. the horizontal cells: Receptive field organisation and response characteristics," *Biological Cybernetics* **46**, pp. 67–79, 1982.
33. D. L. Ruderman, "The statistics of natural images," *Network: Computation in Neural System* **5**, pp. 517–548, 1994.

34. A. van der Schaaf and J. H. van Hateren, "Modelling the power spectra of natural images: Statistics and information," *Vision Research* **36**(17), pp. 2759–2770, 1996.
35. D. L. Ruderman, "Origins of scaling in natural images," *Vision Research* **37**(23), pp. 3385–3398, 1997.
36. E. P. Simoncelli and B. O. Olshausen, "Natural image statistics and neural representation," *Annual Review of Neuroscience* **24**(1), pp. 193–216, 2001.
37. P. L. Clatworthy, M. Chirimuuta, J. S. Lauritzen, and D. J. Tolhurst, "Coding of the contrasts in natural images by populations of neurons in primary visual cortex (v1)," *Vision Research* **43**, pp. 1983–2001, 2003.
38. Y. Petrov and L. Zhaoping, "Local correlations, information redundancy and sufficient pixel depth in natural images," *Journal of Optical Society of America A* **20**(1), pp. 56–66, 2003.
39. D. Abbott, "Focus issue on unsolved problems of noise and fluctuations," *Chaos* **11**(3), pp. 526–538, 2001.
40. R. O. Dror, D. C. O'Carroll, and S. B. Laughlin, "The role of natural image statistics in biological motion estimation," *Proceedings of the IEEE International Workshop on Biologically Motivated Computer Vision,* Seoul, Korea **1811**, pp. 492–501, 2000.
41. D. L. Ruderman and W. Bialek, "Statistics of natural images: Scaling in the woods," *Physical Review Letters* **73**(6), pp. 814–817, 1994.
42. S. Rajesh, D. C. O. Carroll, and D. Abbott, "Elaborated reichardt correlators for velocity estimation tasks," *Proceedings of the SPIE Conference on Biomedical Applications of Micro and Nanoengineering,* Melbourne, Australia **4937**, pp. 241–253, 2002.